Conference on Modelling Fluid Flow (CMFF'18)
The 17th International Conference on Fluid Flow Technologies
Budapest, Hungary, September 4-7, 2018

Development of a Cross-Flow Turbine by using 3D-CFD-Calculations

Christian BODNER[1], Helmut BENIGNI[2], Helmut JABERG[2]

[1] Corresponding author, Institute for Hydraulic Fluid Machinery, Graz University of Technology. Kopernikusgasse 24/4 A-8010 Graz, Phone: +43 (0) 316 873 7573, Fax: +43 (0) 316 873 7577, E-mail: christian.bodner@tugraz.at
[2] Institute for Hydraulic Fluid Machinery, Graz University of Technology. E-mail: helmut.benigni@tugraz.at; helmut.jaberg@tugraz.at

ABSTRACT

This work presents a different approach of developing and optimizing a two chamber-cross-flow turbine by using numerical investigations. The development process starts with the preliminary 1D-calculation of the velocity components to determine the main turbine geometry. Based on the preliminary design a broad-based numerical investigation was conducted by using complex, 2-phase flow calculations with moving surfaces. These investigations implied the whole geometry components of the hydraulic machine (e.g. runner blades, nozzle, guide vane) to determine their influence on the maximum reachable turbine performance. With a simplified CFD-turbine-model, a considerable number of different turbine designs were analyzed. The CFD-calculations clearly show that the major impact on the turbine performance is caused by the runner blades and the interaction between the nozzle and the runner blades.

Following the CFD-calculations, the most promising design was then investigated on a test rig in the laboratory of the Institute for Hydraulic Fluid Machinery. The final step of the development process represents the field measurement of the prototype turbine.

Keywords: CFD-calculations, hydraulic turbine, two phase flow, water turbine;

NOMENCLATURE

D_1, D_2	$[m]$	outer, inner runner diameter
H_t	$[m]$	turbine head
Q	$[m^3 \cdot s^{-1}]$	flowrate
s	$[mm]$	blade thickness
E	$[J \cdot kg^{-1}]$	specific hydraulic energy
F	$[N]$	force
F_{ED}	$[-]$	force factor
T	$[Nm]$	torque
T_{ED}	$[-]$	torque factor
$\vec{c}, c$	$[m \cdot s^{-1}]$	absolute velocity
$\vec{u}, u$	$[m \cdot s^{-1}]$	circumferential velocity
$\vec{w}, c$	$[m \cdot s^{-1}]$	relative velocity
c_u	$[m \cdot s^{-1}]$	circumferential absolute velocity component
g	$[m \cdot s^{-2}]$	gravity
n	$[rpm]$	rotational speed
p	$[Pa]$	pressure
α	$[deg]$	angle of attack
β^*	$[deg]$	blade angle
η	$[-]$	turbine efficiency
λ	$[deg]$	nozzle outlet angle
ω	$[1 \cdot s^{-1}]$	angular velocity
ρ	$[kg \cdot m^{-3}]$	water density

Subscripts and Superscripts

CFD	computational fluid dynamics
CFT	cross-flow turbine
GV	guide vane
abs	absolute
inl, out	inlet, outlet
opt	optimal (at best efficiency point)
tot	total

1. INTRODUCTION

Future trends indicate an increasing impact of small hydro power plants regarding renewable energy technologies [1]. In this case cross-flow turbines (CFT) are widely used in small hydro power plant applications and especially for off-grid-applications. Compared to other turbine types they become more and more notable when it comes to cost effectiveness. The cost effectiveness of CTFs is based on the simple robust design with low maintenance costs. Another advantage in particular with a two-chamber-design is the rather flat efficiency curve over a wide flowrate range. Figure 1 shows the efficiency curve of a two-chamber-CFT compared to a Francis turbine. Though the maximum efficiency of a Francis-turbine is higher than the efficiency of the CFT, at part load the CFT is superior. With the two chamber-design the turbine is split into a 1/3 and a 2/3 cham-

ber. Each of the chambers holds a separate guide vane which allows to adjust the flowrate independently.

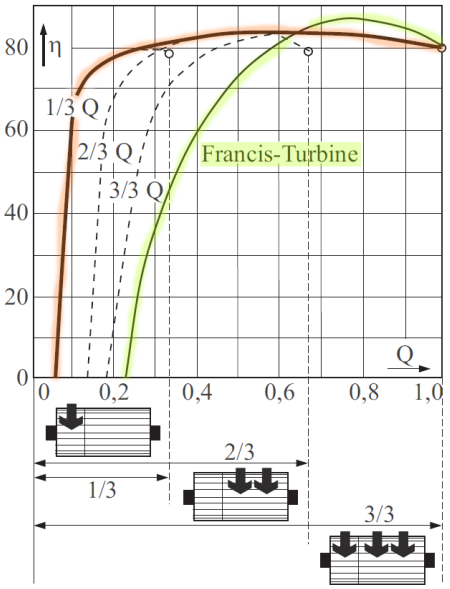

Figure 1. Turbine efficiency of a two-chamber-CFT compared to a Francis-turbine [2]

Figure 2 shows the main parts of the final developed two-chamber-CFT with guide vanes for regulating the flowrate. There are different design-options but the main parts of each CFT are the nozzle and the runner. The nozzle converts the pressure energy into velocity energy and guides the waterjet towards the runner. The runner has a cylindrical shape with radially orientated blades. By redirecting the passing waterjet twice (entering and leaving the runner), the jet-velocity is transferred into torque.

Aside from regulating the flowrate by using the typical guide vane, also known as hydraulic flap (see Figure 6), a sliding guide vane could further improve the turbine performance. The sliding guide vane is positioned between the nozzle outlet and the runner. For regulating the flowrate, it could be rotated circumferential around the runner and reduces the outlet area of the nozzle. As a result of positioned outside the flow field of the nozzle the head loss is lower than with a hydraulic flap. Contra wise to the minor head loss the sliding guide vane is more complex to implement and operate.

For low head turbine applications a draft tube could be attached to utilize a maximum of the given head. With an attached draft tube the waterjet mixes with the air inside the turbine housing and as a result the air is carried out of the turbine and induces a depression inside the turbine housing. Due to the depression the water column inside the draft tube rises above the tail water level. To adjust the water level inside the draft tube and to prevent the runner filling up with water, a air-suction-valve is placed at the back of the turbine housing. Furthermore, the position of the air inlet valve could have positive effects on the turbine performance. [3]

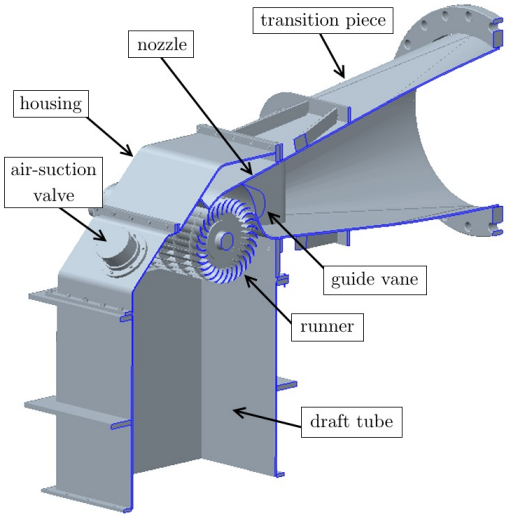

Figure 2. Main parts of a two-chamber-CFT

Typically, the development and improvement-process of CFTs is characterized by using cost and time intense experimental investigations. *Mockmore & Merryfield* carried out the first test rig developments for CFTs in 1949 [4]. More recent test rig investigations were performed by *Khosrowpanah* [5], *Fiuzat & Akerkar* [6] and *Desai* & Aziz [7][8]. The main focus of such experimental investigations is to determine the impact on main turbine parameters like the turbine efficiency by changing geometry parts (e.g. nozzle, blade) of the turbine. Years ago, numerical simulations were not state of the art in developing a CFT. However, nowadays numerical investigations have become more noticeable. Major investigations by using numerical calculations have been done by *Sammartano* [9] [10], *Chen* [11] and *Kaunda* [12].

2. PRELIMINARY DESIGN AND NUMERICAL SIMULATION

The preliminary turbine design was fixed by using the Euler-equation for turbo-machinery and guidelines from *Mockmore & Meryfield* [4], *Nasir* [13], *Sammartano* [9, 10] and *Giesecke* [2]. Due to the fact that the water jet passes the runner twice (see Figure 3) the turbo-machinery equation for CFTs can be written as follows:

$$H_t = \frac{1}{g} \cdot \left[\overbrace{(u_1 \cdot c_{u1} - u_2 \cdot c_{u2})}^{1st\ \ stage} + \overbrace{(u_3 \cdot c_{u3} - u_4 \cdot c_{u4})}^{2nd\ \ stage} \right] \tag{1}$$

By using the Euler-equation the blade inlet- and outlet-angles were calculated. To ensure a maximum power output, a swirl free outflow at the outlet of the second turbine stage (index 4) is assumed. Therefore

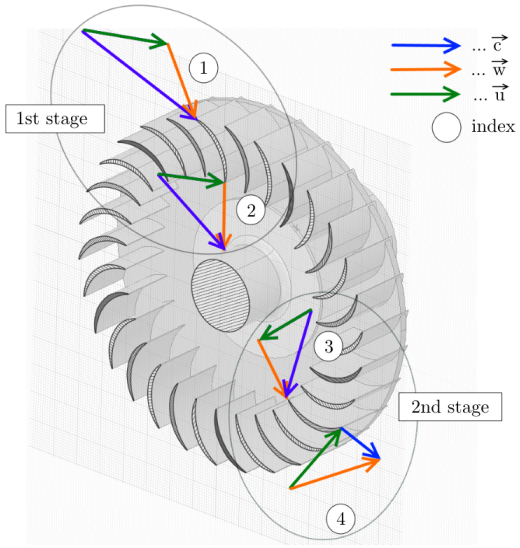

Figure 3. Velocity triangles of the CFT for each turbine stage

the $(u_4 \cdot c_{u4})$ is equal to zero. Another simplification in case of no losses inside the runner was introduced by *Sammartano* [9]. Without losses the velocity triangles at the outlet of the first stage (index 2) and the inlet of the second stage (index 3) are equal, therefore, they can be cancelled out. As a result, the flow conditions at the inlet of the first turbine stage are decisive for the turbine blade-design.

Figure 4 shows the velocity triangle at the inlet of the first stage. The most important parameter of designing the turbine is the angle of attack α (see Fig.4 and Figure 7), which is set by the nozzle shape. To maximize the power output of the turbine, the angle of attack should be as small as possible. Due to a minor α-angle the circumferential absolute velocity component c_u increase (see Fig.4) and related to the turbo-machinery equation the turbine power output is raised. By reason of manufacturing-limitations a common angle of attack is $\alpha = 16°$. [14]

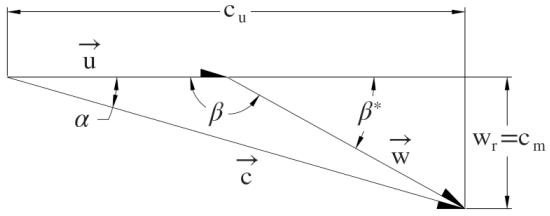

Figure 4. Velocity triangle at the inlet of the first stage

The given data and the main basic turbine parameters of the final turbine design are summarized in Table 1.

2.1. CFD-Model and Setup

Based on the preliminary design a turbine-model was created by using ANSYS DesignModeler. To

Table 1. Nominal operation data and main design parameters of the turbine

Parameter	Dimension	Unit
H_t	12,0	m
Q_{opt}	1,0	m^3/s
n	300	rpm
α	16	deg
β^*	29,8	deg
D_2/D_1	0,68	–

reduce the computing time of the complex transient two-phase-flow calculations the turbine model was simplified. This simplified turbine model measures one-tenth of the original turbine-width. The width mainly influences the flowrate of the CFT while the influence on the turbine efficiency is negligible. Despite the fact of the reduced width it is possible to get reliable and realistic results regarding the turbine characteristics.[9, 10] Due to the complex modelling of the draft tube effect with the air suction valve, the head recovery of the draft tube was assumed and added to the given head at the turbine inlet.

The simplified turbine-model was divided into separate parts (domains) like nozzle, connector, runner, inner runner and housing (Figure 6). For each domain a hexadron-mesh was generated by using ANSYS Meshing. In course of a mesh size study it turned out that the mesh density shown in Table 2 is sufficient to reach mesh-independent results for the turbine characteristics. A visualization of the CFD-meshes of the turbine model is shown in Figure 5.

Table 2. Overview of the mesh sizes used

Domain	Nodes	Elements
Nozzle	89.000	76.800
Connector	18.600	8.300
Runner	419.000	355.100
Inner runner	53.000	46.500
Housing	13.800	116.100

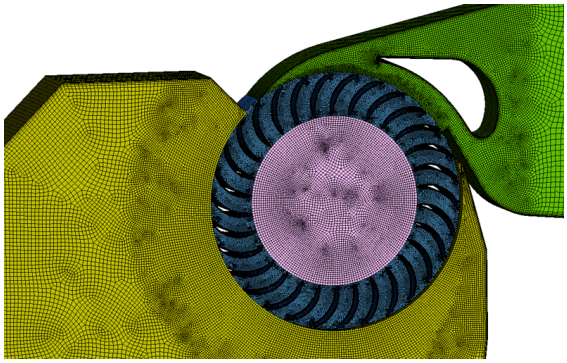

Figure 5. Visualization of the meshes created for each component of the turbine

For creating the CFD-model, the simulation process and the evaluation of the CFD-results, the com-

mercial software package ANSYS-CFX V17.1 was used. Fig.6 shows the CFD-setup of the CFT with the guide vane for regulation. To model the two-phase-flow, the *standard free surface homogeneous model* was used. In this both fluids share the same flow- and turbulence-field. All simulation were carried out with the Shear-Stress-Transport turbulence model for Scale Adaptive Simulations (SST-SAS).

For the boundary condition at the turbine inlet the total pressure $p_{tot,in}$ (including the head recovery of the draft tube) with the volume fraction of 1 for water and 0 for air (100% water, 0% air) was set. At the turbine outlet an opening with an absolute pressure of $p_{abs,out} = 1bar$ and a volume fraction of 0 for water and 1 for air (0% water, 100% air) was set. The connection between the connector and runner domain as well as between the runner and inner runner domain was set as *transient rotor stator*.

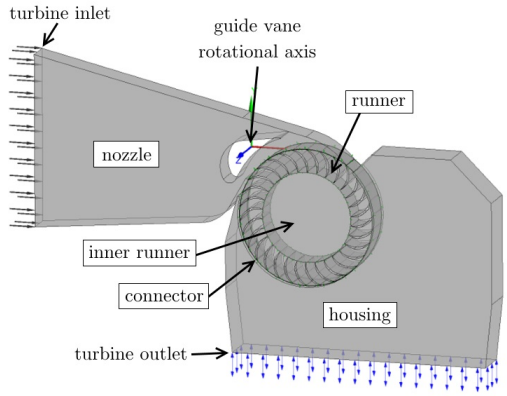

Figure 6. CFX-Pre setup of the CFD-turbine-model

All calculations were carried out until at least 10 revolutions of the runner were computed. Based on a timestep investigation, the transient timestep was chosen in a way to reach an angular resolution of $\Delta\varphi = 2°$ per iteration. Further reduction of the timestep does not contribute to reach improved turbine characteristic results. To determine the turbine characteristics, the mean values of the last 5 revolutions were used.

According to the IEC standards [15] the turbine efficiency is defined as follows:

$$\eta = \frac{T_{runner} \cdot \omega}{\rho \cdot g \cdot Q \cdot H_t} \tag{2}$$

The net head H_t represents the difference between the static pressure at the inlet and the static pressure at the outlet where the mean kinetic energy head is added to the inlet and outlet pressures. The outlet of the turbine without a draft tube is located at the rotational axis level with an outlet velocity of $v_{out} = 0$ and an outlet pressure of $p_{out} = p_{atm} = 1bar$. [15]

2.2. CFD-Results

As mentioned, the important parts, which are responsible for achieving a good turbine efficiency are the nozzle and the runner blades. Regarding the nozzle the angle of attack α, and the type of regulating the flowrate is important. Therefore, investigations regarding the angle of attack and two different types of regulating the flowrate were carried out. Figure 7 shows the nozzle shapes with the sliding guide vane and different angle of attack ($\alpha = 16°$ and $\alpha = 20°$). The nozzle outlet angle $\lambda = 90°$ of both designs is equal, so the only difference is related to the upper wall shape. Caused by the greater angle of attack, the upper wall shape of the $\alpha = 20°$-nozzle is slightly higher. Additionally the design of the nozzle with the hydraulic flap is marked. The hydraulic-flap-nozzle has an 16° angle of attack and a nozzle outlet angle of $\lambda = 100°$.

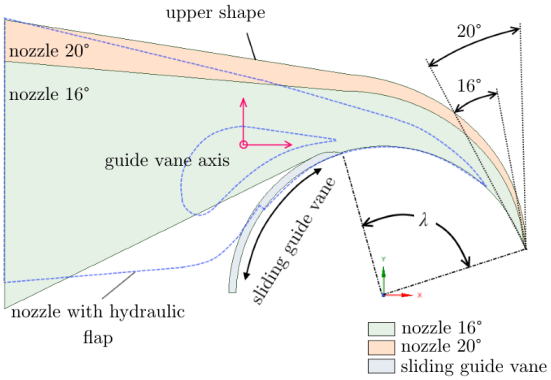

Figure 7. Nozzle with sliding guide vane and hydraulic flap for regulating the flowrate

For each angle of attack the blade inlet angle β^* was adopted to ensure shock less approach flow towards the first turbine stage. Figure 8 shows the efficiency curves of the different nozzle designs. Regarding angle of attack α (sliding-guide-vane-nozzle), it can be shown that a flatter angle leads to a higher turbine efficiency.

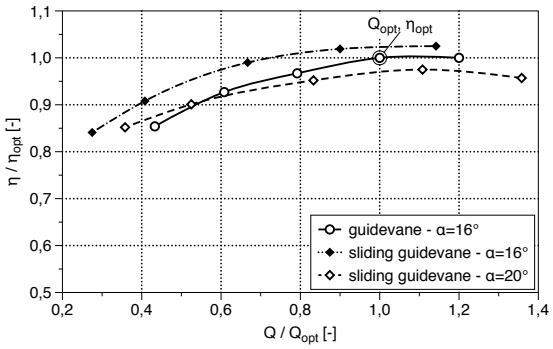

Figure 8. Turbine efficiency of the nozzle with sliding guide vane and the hydraulic flap

Related to equation (1) and Figure 9 the circumferential velocity with flatter angle of attack $\alpha = 16°$

is higher. With a higher circumferential velocity the product $u \cdot c_u$ is higher and H_t increases, thus the turbine power increases. In contrast, a higher angle of attack ($\alpha = 20°$) implies a higher radial velocity w_r, therefore the flowrate of the turbine is higher compared to a lower angle of attack ($\alpha = 16°$).

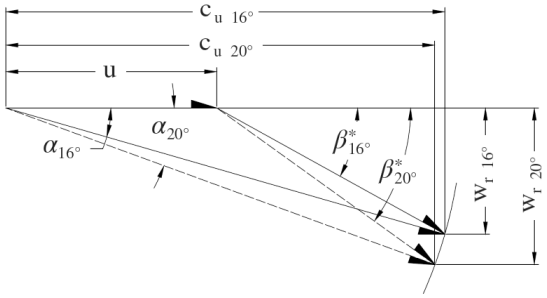

Figure 9. Velocity components for different angle of attack

In comparison to the sliding guide vane (equal $\alpha = 16°$), the turbine efficiency of the hydraulic flap is lower because it is positioned inside the flow field of the nozzle and therefore the head loss of the nozzle is higher. Additionally aside the best operation-point-position of the hydraulic flap, the velocity distribution is very inhomogeneous. Especially at nearly closed position the approaching flow towards the runner is strongly influenced by the hydraulic flap position. Despite the lower efficiency, the hydraulic flap was chosen for the final turbine design. The main reason is that the hydraulic flap has a closing-tendency. This means that if the turbine or the fixation of the guide vane fails, it automatically closes because of the hydraulic torque caused by the flow field.

Figure 10 shows the torque factor T_{ED} and the radial force factor F_{ED} of the chosen hydraulic flap design (shown in Fig.7) over different nozzle openings. For determining the force and torque of the guide vane, additional stationary one-phase-calculations, without runner and housing domain were performed. These forces and torques are needed for the basic turbine-design-concepts of the turbine model and the prototype turbine. The torque- and force-factor is calculated regarding the IEC-standards [16]:

$$F_{ED} = \frac{F}{\rho \cdot D_1^2 \cdot E} \tag{3}$$

$$T_{ED} = \frac{T}{\rho \cdot D_1^3 \cdot E} \tag{4}$$

With the chosen design, the torque which is caused by the flow field is positive along the entire opening range. Related to the guidvane coordinate system (shown in Fig.7) a positive torque factor implies a closing tendency, so the guide vane automatically closes in case of failure. At nearly closed position the force factor of the guide vane reaches a maximum and at higher guide vane openings the force factor decreases.

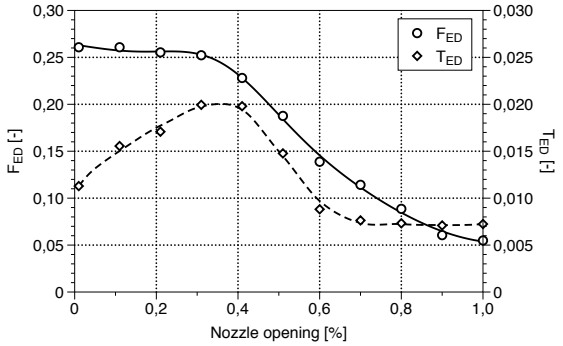

Figure 10. Torque- and force-factor of the hydraulic flap at different nozzle openings

As noted before the runner blades have a huge effect on the turbine efficiency. Therefore, three general runner blade designs were investigated (Figure 11). Two of the profiles have a constant blade thickness of $s = 6mm$ along the blade length, only the inlet and outlet edges have different shapes. Both have a rounded trailing edge at the inner diameter. At the outer diameter one blade has an angled leading edge and the other one a rounded leading edge. The third one is a profiled blade design, which means the thickness along the blade varies and the leading- and trailing-edge is tapered. The investigation of the blade profiles was performed with the hydraulic flap nozzle shown in Fig.7. The inlet- and outlet angles of all three blade designs were kept constant.

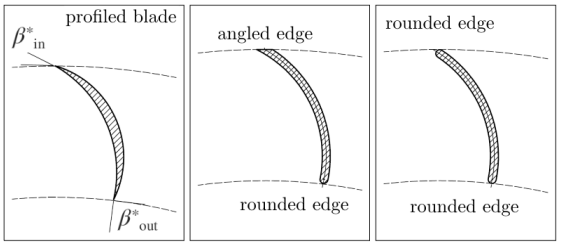

Figure 11. Different runner blade designs

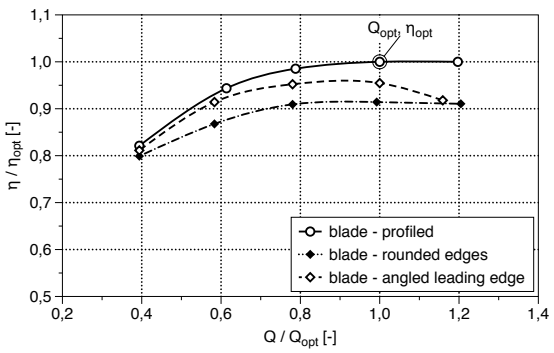

Figure 12. Turbine efficiency of the different runner blade designs

Figure 12 shows the reached turbine efficiency of the different runner blade designs. It points out that the profiled blade design leads to a higher turbine efficiency. The main reason is the sharper leading- and trailing edge. Sharper inlet- and outlet-edges are superior because the shock-loss is lower than with rounded edges. However, this only applies when the flow towards the blades and the blade inlet angle are coincident. Vice versa sharper blade edges could result higher losses if the flow direction and the blade inlet angle are not coincident.

In order to understand the energy transformation of the different blade designs a detailed analysis of the transferred torque was carried out. For each blade design the torque factor of a single blade during one revolution of the runner at full guide vane opening ($Q/Q_{opt} = 1,2$) is shown in Figure 13. Each blade enters the waterjet at a blade rotation of $\sim 30°$. After entering the water jet the transferred torque increases until the bladed is near the nozzle tip ($\sim 165°$). At a blade rotation of $\sim 170°$ the water jet changes the flow-direction inside the blade channels and the torque is nearly equal to zero. After the blade leaves the waterjet at the second turbine stage (blade rotation $\sim 270°$) the torque is again equal to zero and no torque is transferred until the blade enters the waterjet at the first turbine stage again. In addition to the torque factor the accumulated torque factor $\sum T_{ED}$ is shown. Considering the accumulated torque factor, it points out that the profiled blade reaches the maximum of torque transmission during one rotation of the runner. The two blade designs with the constant blade thickness are achieving equal torque production during one revolution.

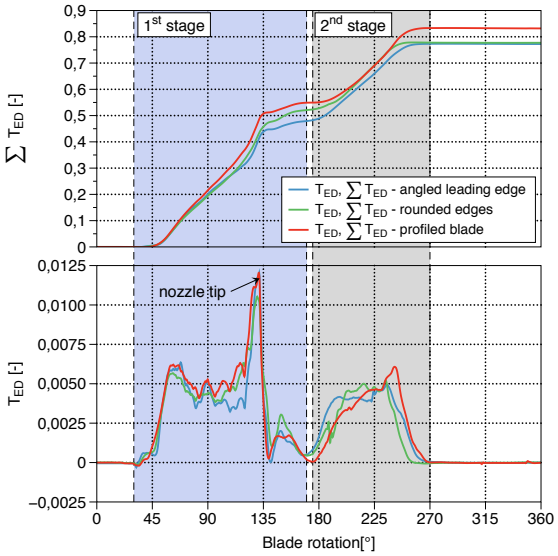

Figure 13. Torque factor and accumulated torque factor of a single blade across one revolution of the runner

Out of the accumulated torque factor, Figure 14 shows the distribution of the torque by each turbine stage. For the blade designs with constant blade thickness the distribution between the first and the second turbine stage is 70% to 30%. With the profiled blade design the contribution of the second turbine stage is higher during one revolution (66% to 34%).

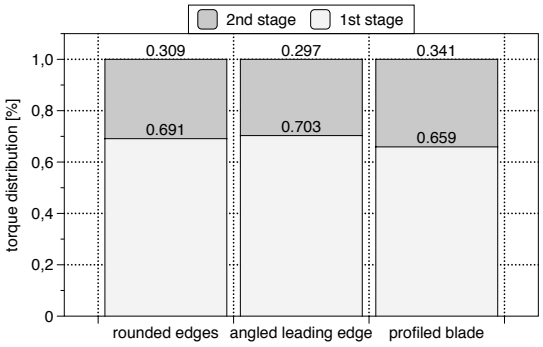

Figure 14. Torque distribution of the two turbine stages of the three different blade designs

It can be summarized that the profiled blade design with pointed leading and trailing edge is superior. Concerning the torque distribution, the first turbine stage is more important than the second turbine stage. Nevertheless, optimizing the first turbine stage consequently influences the performance of the second turbine stage.

3. EXPERIMENTAL AND PROTOTYPE MEASUREMENTS

Due to the fact of using a simplified CFD-model, it is essential to prove the optimization results of the complex 2-phase transient flows in course of experimental measurements. Therefore, a turbine model with a scale factor of 1:2 was engineered and tested on the 4-quadrant test rig. Figure 15 and figure 16 show the 3D-design of the turbine model at the 4-quadrant test rig. By only considering the draft tube effect at inlet-boundary condition in the CFD-calculations, one of the focus-points of the experimental investigations is related to the effect of the draft tube. Hence a tail water basin was installed, which allows to adjust different tail water levels. The turbine was placed on a steel structure above the tail water basin and the draft tube of the turbine is extended into the tail water basin. The air suction valve was placed at the back of the turbine housing (Fig.16). With the air suction valve the depression inside the turbine housing and therefore the height of the water column inside the draft tube could be adjusted. The nozzle is connected via the transmission piece with the pressure pipe of the test rig. Between the generator and the turbine shaft a torque transducer is placed. All measurements were carried out regarding the IEC standards [16, 15]. The measurement hardware is based on a modular system (National Instruments - NI-CDaq) coupled with an inhouse designed measurement software based on Labview. Every operation point is measured over a period of $t = 30sec$ with a sample rate of $1kHz$. Out

of these 30000 values the arithmetic mean value is calculated. In Table 3 the measurement categories and the used measurement equipment for the test rig measurements are listed.

Table 3. Measurement categories and equipment

Physical value	Equipment
Flowrate	ABB FSM4000
Differential pressure	Rosemount 3051 CD4
Absolute pressure	Rosemount 3051 CA2
Torque, runner speed	HBM T30
Temperature	Volton PT100

With the systematic uncertainties (Table 4) and random uncertainty of $\pm 0,15\%$ (based on the determined repeatability) the total uncertainty of the measured efficiency accounts for $\pm 0,406\%$.

Table 4. Systematic measurement uncertainties

Physical value		Uncertainty
Flowrate	Q	$\pm 0,331\%$
Turbine head	H_t	$\pm 0,141\%$
Torque	T	$\pm 0,1\%$
Runner speed	n	$\pm 0,05\%$

Generally the IEC standards differentiate between two cases for measuring a CFT: One without the draft tube and one case with attached draft tube. The only difference is therefore the definition of the turbine outlet. As mentioned before without the draft tube the outlet is defined by the level of the rotation axis with atmospheric pressure and the outlet velocity of $c_{out} = 0$. For measurements with attached draft tube the outlet of the turbine is defined by the tail water level and the outlet velocity is set by the flowrate Q and the cross section of the draft tube outlet.

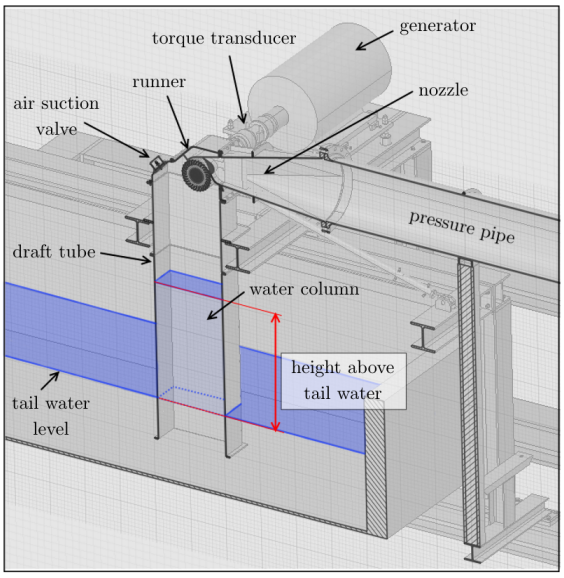

Figure 15. 3D-design of the turbine test rig

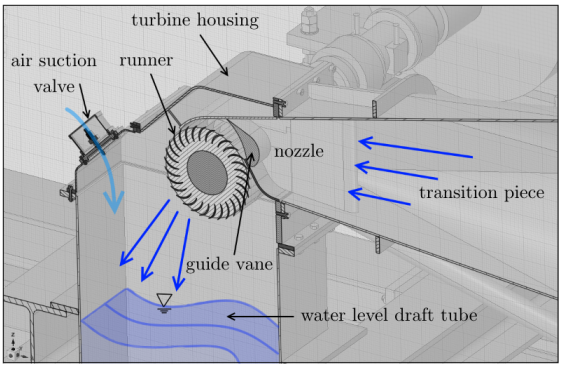

Figure 16. Detail of the test rig model turbine

Figure 17 shows the turbine efficiency at different guide vain openings (3/3 turbine chamber width) with and without head-recovery of the draft tube. Without head recovery, the air suction valve at the back of the turbine housing is fully opened. As a result, there is no depression inside the turbine housing and the water level inside draft tube is equal to the tail water level. In contrast to no depression, a maximum reachable depression is realized by adjusting the air suction valve. The maximum depression inside the draft tube is restricted by the demand of preventing the water column of floating the runner. With the developed suction valve (fixed position) the height of the water column above the tail water level is nearly constant over the different guide vane openings ($H_{drafttube}/H_{opt} \approx 0,065$).

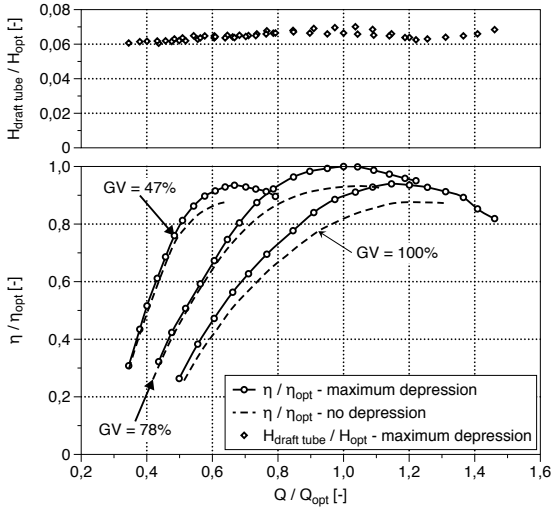

Figure 17. Influence of the draft tube on the turbine efficiency at different guide vane openings (3/3 turbine chamber width)

Fig.17 implies a significant influence of the draft tube and the regulated depression inside the housing on the turbine efficiency. Therefore, adjusting the air suction valve at turbines with draft tube is indispensable to guarantee a maximum utilization of the head between the runner outlet and the tail water level.

Subsequent to successful test rig measurements

the prototype turbine was taken into operation. After a running-in period the prototype turbine characteristics were measured to verify the development and optimization process. The turbine characteristics of the final two chamber prototype turbine is shown in Figure 18.

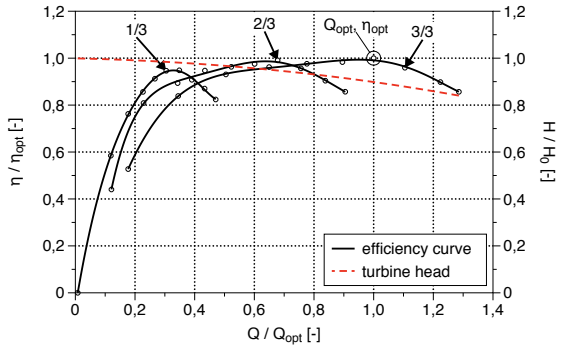

Figure 18. Turbine characteristics for 1/3, 2/3 and 3/3 chamber operation of the prototype turbine.

Compared to Fig.1 the overall turbine efficiency curve of the prototype turbine confirms the rather flat trend between $Q/Q_{opt} = 0,3-1,1$, thus the turbine is appropriate to handle highly varying flow rates. The turbine head curve is given by the power house environment (pressure pipe, valve) and strongly decreases at higher flowrates. However the maximum reached turbine efficiency of the 2/3 and 3/3 turbine chamber are almost identically. Hence the turbine is also able to handle varying head to a certain extent without effecting the turbine efficiency.

4. SUMMARY

The current study presents the overall development of a cross-flow turbine by using 3D-CFD-calculations for determining the ideal geometry of the turbine. Based on the preliminary design a large number of different geometry variations was analyzed. During the CFD-optimization it turned out that the shape of the nozzle and the runner blade design have a major impact on the turbine characteristics. Related to the nozzle design, the investigation exhibits, that the angle of attack and the guide vane type are important to reach an improved efficiency curve. Although the turbine design with a sliding guide vane results in a higher turbine efficiency, the hydraulic flap design brings additional safety in case of a turbine failure. Beside the nozzle design, the shape of the runner blade is important to achieve an excellent turbine efficiency. The investigations clearly point out, that profiled blades with pointed leading- and trailing-edge are superior and yields a higher turbine performance. Despite the fact of the simplified CFD-turbine model, the turbine measurements confirmed the CFD-optimization results.

Despite of its simplicity, the two-phase-flow conditions inside the turbine are highly challenging and test rig measurements are essential. Hence the daft tube effect could only be investigated at the test-rig. It could be shown, that the draft tube has an significant impact on the turbine performance for low head applications.

REFERENCES

[1] Kelly-Richards, S., Silber-Coats, N., Crootof, A., Tecklin, D., and Bauer, C., 2017, "Governing the transition to renewable energy: A review of impacts and policy issues in the small hydropower boom", *Energy Policy*, Vol. 101 (November 2016), pp. 251–264.

[2] Giesecke, J., and Mosonyi, E., 2009, *Wasserkraftanlagen*, Springer Berlin Heidelberg, Berlin, Heidelberg, 5. auflage edn., ISBN 978-3-540-88988-5.

[3] Choi, Y. D., Yoon, H. Y., Inagaki, M., Ooike, S., Kim, Y. J., and Lee, Y. H., 2010, "Performance improvement of a cross-flow hydro turbine by air layer effect", *IOP Conference Series: Earth and Environmental Science*, Vol. 12, p. 012030.

[4] Mockmore, C. A., and Merryfield, F., 1949, "The Banki Water Turbine", *Tech. rep.*, Oregon State College, Corvallis.

[5] Khosrowpanah, S., 1988, "Experimental study of cross-flow turbine", *Journal of Hydraulic Engineering*, Vol. 114 (3), pp. 299–314.

[6] Fiuzat, A., and Akerkar, B., 1989, "The use of interior guide tube in cross flow turbines", *Waterpower'89*, pp. 1111–1119.

[7] Desai, V., and Aziz, N., 1994, "An experimental investigation of cross-flow turbine efficiency", *Journal of Fluid Engineering*, Vol. 116 (September), pp. 545–550.

[8] Desai, V., and Seshadri, V., 1996, "Parametric study on performance of cross-flow turbine(a)", *Journal of energy engineering*, Vol. 122 (1), pp. 126–127.

[9] Sammartano, V., Aricò, C., Carravetta, A., Fecarotta, O., and Tucciarelli, T., 2013, "Banki-Michell Optimal Design by Computational Fluid Dynamics Testing and Hydrodynamic Analysis", *Energies*, Vol. 6 (5), pp. 2362–2385.

[10] Sammartano, V., Arico, C., Sinagra, M., and Tucciarelli, T., 2015, "Cross-Flow Turbine Design for Energy Production and Duscharge Regulation", *Journal of Hydraulic Engineering*, Vol. 141 (March 2015).

[11] Chen, Z. M., and Choi, Y. D., 2013, "Performance and internal flow characteristics of a cross-flow turbine by guide vane angle", *IOP Conference Series: Materials Science and Engineering*, Vol. 52 (5), p. 052031.

[12] Kaunda, C., 2014, “A numerical investigation of flow profile and performance of a low cost Crossflow turbine”, *International Energy and Environment Foundation*, Vol. 5 (3), pp. 275–296.

[13] Nasir, B., 2013, “Design of High Efficiency Cross-Flow Turbine for Hydro-Power Plant”, *International Journal of Engineering and Advanced . . .* , (3), pp. 308–311.

[14] Kaunda, C., Kimambo, C., and Nielsen, T., 2014, “Experimental study on a simplified crossflow turbine”, *Energy and Environment*, Vol. 5 (2), pp. 155–182.

[15] International Electrotechnical Commission, 2010, “IEC62006”, .

[16] International Electrotechnical Commission, 1999, “IEC 60193”, .